EPJ Web of Conferences **84**, 05001 (2015)
DOI: 10.1051/epjconf/20158405001

Production of a rovibrationally selected O_2^+ beam for dissociative recombination studies

A. Dochain[a] and X. Urbain

Institute of Condensed Matter and Nanosciences, Université catholique de Louvain, Chemin du cyclotron 2, 1348 Louvain-la-Neuve, Belgium

Abstract. In order to study the reactivity of particular excited states of O_2^+, we have studied the resonance enhanced multiphoton ionization of O_2 via the $^{1,3}\Pi_g$ states with a frequency-doubled pulsed dye laser in the range 296.5–303.5 nm. We managed to produce a large ensemble of O_2^+ ions in selected v^+, N^+ states, with $v^+ = 0$ or 1, and N^+ up to 25. Such an ion source, with tunability and selectivity of the output rovibrational state, can be coupled to a storage device in order to study the collisional and radiative properties of infrared inactive species.

1. Introduction

The dissociative recombination (DR) of O_2^+ has been extensively studied, for its contribution to the green airglow [1], and its sensitivity to vibrational excitation [2]. Petrignani *et al.* [3] have developed and characterized an electron impact source, which was installed at the CRYRING storage ring to study the vibrational dependence of the DR rate coefficient through a decomposition of the projected distance spectra recorded under different source conditions. In this paper an alternative method for the production of a rovibrationally selected beam of O_2^+ is discussed, which relies on resonance enhanced multiphoton ionization (REMPI) of a gas jet in a dedicated laser ion source.

The key feature of the present study is the selection an intermediate state with narrow linewidth, allowing us to precisely select the rovibrational level coming into resonance. The Rydberg character of that intermediate state ensures the conservation of the vibrational quantum number upon ionization, while rotation may only be affected by the angular momentum imparted to the photoelectron.

In this case, we chose the $O_2(d\ ^1\Pi_g)$ Rydberg state associated to the ground state of the ion $O_2^+(X\ ^2\Pi_g)$, which is easily accessed by a two-photon transition and ionized by the absorption of an additional photon in a (2+1) REMPI sequence:

$$O_2(X\ ^3\Sigma_g^-, v = 0, N) + 2\gamma(\sim 300\ \text{nm}) \rightarrow O_2(d\ ^1\Pi_g, v', N') \quad (1)$$

$$O_2(d\ ^1\Pi_g, v', N') \quad + \gamma \rightarrow O_2^+(X\ ^2\Pi_g, v^+, N^+) + e^-. \quad (2)$$

[a] Corresponding author: arnaud.dochain@uclouvain.be

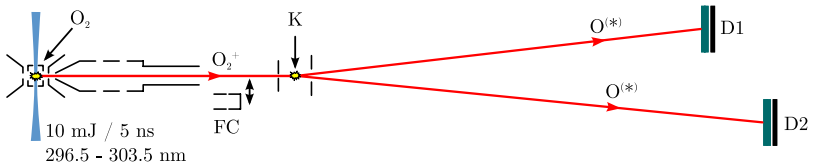

Figure 1. Experimental setup. FC: Faraday cup; D1, D2: position sensitive detectors; K: effusive potassium jet.

Rovibrational state selectivity was verified experimentally, using in the first case a simulation of the wavelength-dependent ion yield for a close comparison to the experimental spectrum, and in the second case by measuring the kinetic energy release (KER) upon dissociative charge transfer with an effusive potassium jet.

2. Experimental setup

The experimental setup used for creating and analyzing the selected O_2^+ beam is shown in Fig. 1. The ionization and analysis stages are the following:

An effusive jet of O_2 is injected in the ionization chamber, where it may be ionized by an ion beam or a laser beam. In the present study, radiation in the range 296.5–303.5 nm was generated by frequency doubling the output of a tunable dye laser pumped by a Nd:YAG laser (5 ns, 0.1 cm^{-1} FWHM) at a repetition rate of 30 Hz. A set of electrodes accelerates O_2^+ outside the chamber with a given speed and direction. Typical acceleration voltages are in the range from 2 to 8 keV.

For a measurement of the total yield, the intensity of the O_2^+ beam can measured in a retractable Faraday cup. For internal state analysis, the beam interacts further downstream with an effusive potassium jet. Dissociative charge exchange (DCE) occurs and two oxygen atoms are released with a given kinetic energy in the center-of-mass frame. The KER is measured with two position-sensitive detectors D1 and D2 operating in coincidence. Both detectors are made of microchannel plates placed in front of a resistive anode for position encoding. Three-dimensional imaging is performed to retrieve the kinetic energy by iteratively solving the equations of motion.

3. Intermediate state

The first step for the production of a beam by REMPI is the proper characterization of the resonant state involved. The two-photon absorption spectrum is affected by the detailed rotational structure of the ground and excited states of O_2. Unambiguous identification of the transitions is crucial to ensure proper selection of a specific state of the ion.

3.1 Nuclear spin effect

To have a better understanding of the selection rules affecting the rotational transitions it might be useful to conduct a deeper investigation of the ground state of $^{16}O_2$ and the nuclear spin effect due to the symmetry of this homonuclear diatomic molecule.

Let us begin with its total molecular wave function, which may be factorized as follows:

$$\psi_{\mathrm{mol}} = \psi_{\mathrm{el}} \frac{\psi_v}{R} \phi_N \chi_{\mathrm{el}}.$$

The oxygen ground state is a $^3\Sigma_g^-$ state. Therefore, the total wave function ψ_{mol} is symmetric (because ^{16}O nuclei have a spin of 0 and so are bosons), the electronic wave function ψ_{el} is antisymmetric, the purely radial part of the molecular wave function ψ_v/R is by definition always symmetric, and the wave

function of the electrons χ_{el} is by definition always antisymmetric. Consequently, the wave function of the angular momentum of the nuclei apart from spin ϕ_N must be symmetric, thus only even values of N are possible [7].

3.2 Non-degenerate levels of (O_2) ground state

The ground state of O_2 is a triplet state, leading to three slightly non-degenerate levels with energy given by:

$$F_1(N) = B_v N(N+1) + (2N+3)B_v - \lambda - \sqrt{(2N+3)^2 B_v^2 + \lambda^2 - 2\lambda B_v} + \gamma(N+1)$$

$$F_2(N) = B_v N(N+1)$$

$$F_3(N) = B_v N(N+1) - (2N-1)B_v - \lambda + \sqrt{(2N-1)^2 B_v^2 + \lambda^2 - 2\lambda B_v} - \gamma N$$

with F_1, F_2 and F_3 corresponding to $J = N+1$, $J = N$ and $J = N-1$ respectively, where $\lambda = 1.984$ and $\gamma = -0.0084$ are constants, and $B_v = 1.43777\ \mathrm{cm}^{-1}$ is the rotational constant for $O_2(X\,^3\Sigma_g^-, v = 0)$ [7].

3.3 Selection rules

In order to establish the selection rules governing the two-photon transition, one must specify to which Hund's case the states involved in the REMPI process are associated, and identify the appropriate quantum number for the rotational transition.

The ground state of the molecule is a $^3\Sigma_g^-$ state. It is better described by Hund's case (b), while the intermediate state is a Rydberg state, described by Hund's case (e) [8]. Thus, the only good quantum number that can be used for this transition is N, the total angular momentum apart from spin [9].

Although the selection rules for the excitation with two photons apply only to the total angular momentum $J' = J, J \pm 2$, the only good quantum number that characterizes this transition is $N = J, J \pm 1$, so the allowed rotational transitions are $N' = N, N \pm 1, N \pm 2, N \pm 3$ [5].

By scanning the wavelength, it is possible to observe all rovibrational transitions between the ground and Rydberg states. There are seven rotational branches (Fig. 2) referred to as N, O, P, Q, R, S, T, corresponding to $N' = N-3,\ N-2,\ N-1,\ N,\ N+1,\ N+2,\ N+3$, respectively, which are further divided into twenty-one components due to the non-degeneracy of the triplet ground state of the molecule.

3.4 Line shape and intensity

The transition probabilities among the various rotational levels depend on the degeneracy and Boltzmann factors [7]:

$$p_i(N, N') \sim \left(N + N' + 1\right) \exp(-F_i(N)/kT)$$

with a temperature $T = 300\,\mathrm{K}$ and k the Boltzmann constant. Each peak is given a Lorentzian shape with a linewidth of $1.7\ \mathrm{cm}^{-1}$ compatible with those found by Sur *et al.* [5] and Li *et al.* [10].

A naive simulation has been made using the Boltzmann rotational distribution at 300 K and a constant Lorentzian profile for each transition (Fig. 3). The good overall agreement shows that we are indeed able to select a specific rotational level, provided one can resolve the contribution of different rotational branches. In a subsequent analysis of the internal state of O_2^+, we will assess the vibrational and rotational selectivity of the ionization step.

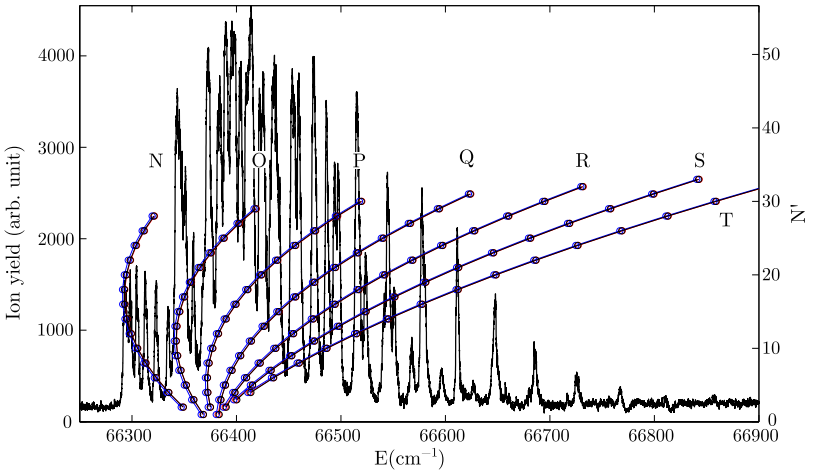

Figure 2. Assignment of rotational transitions between X $^3\Sigma_g^-$, $v = 0$ and d $^1\Pi_g$, $v' = 0$ states of O_2. Solid black line: Experimental spectrum, red-blue-black curves and circles: fortrat parabolas for all rotational branches and spin components F_1, F_2, F_3 respectively.

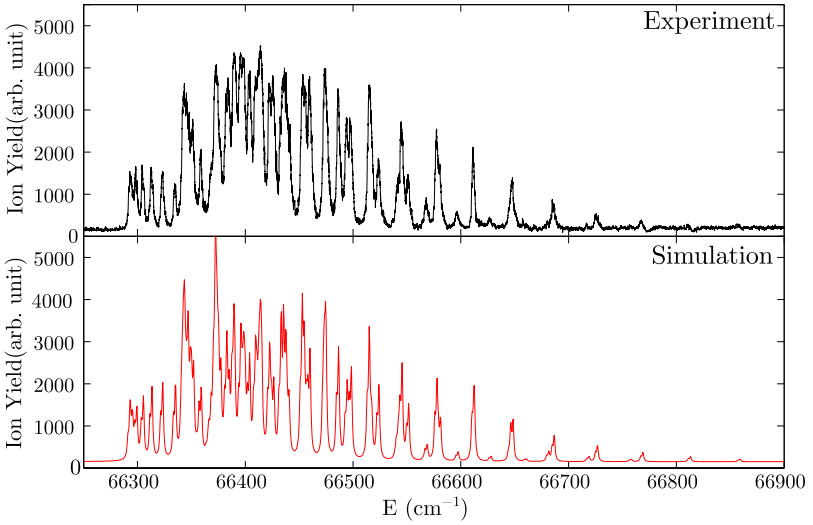

Figure 3. Experimental (top) and simulated (bottom) spectra of the (2+1) REMPI of O_2 between 298 and 301 nm.

4. Kinetic energy release analysis of the internal excitation of O_2^+

The dissociative charge exchange with an alkali-metal target has been extensively studied for O_2^+ by van der Zande *et al.* [4]. Two different dissociative charge exchange processes (DCE) are present, direct (DDCE) and indirect (IDCE) (Fig. 4), each of them producing a characteristic KER spectrum.

To explain DDCE, let us first consider the squared modulus of the wave function of the vibrational state as a function of internuclear distance R. The ion is neutralized by electron transfer from the potassium atom to a dissociative state of the neutral molecule. This process is fast enough to preserve the internuclear distance between the two oxygen atoms. Then, the molecule dissociates with a KER related to the energy difference between the potential energy of this dissociative state at the internuclear distance of the neutralization and its asymptotic limit. Assuming that the dissociative curve is linear, the

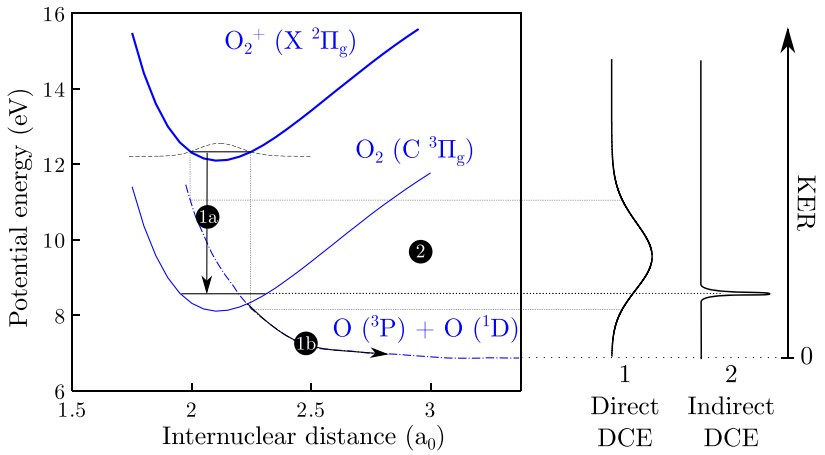

Figure 4. Schematic representation of DCE. Indirect DCE (1): the ion (thick blue line) is neutralized to a Rydberg state (1a) (thin blue line). Coupling to a valence state (dash-dotted blue line) leads to dissociation (1b). Direct DCE (2): the ion is directly neutralized to the valence state.

Table 1. Franck-Condon factors governing both the photoionization of the d $^1\Pi_g$ state and the IDCE process.

FCF(v^+, v')		O_2(d $^1\Pi_g$)					
		0	1	2	3	4	5
O_2^+(X $^2\Pi_g$)	0	0.9998	0.0000	0.0001	0.0000	0.0000	0.0000
	1	0.0000	0.9995	0.0000	0.0004	0.0001	0.0000
	2	0.0001	0.0000	0.9989	0.0000	0.0007	0.0001
	3	0.0000	0.0004	0.0000	0.9981	0.0000	0.0011
	4	0.0000	0.0001	0.0007	0.0000	0.9972	0.0000
	5	0.0000	0.0000	0.0001	0.0012	0.0000	0.9960

KER spectrum associated to DDCE is a projection of the vibrational wave function of the ion, producing Gaussian-like peaks for $v^+ = 0$ ions.

In the IDCE process, the electron is captured into a Rydberg state (quasi resonant with the potassium IP). This reaction redistributes the rovibrational population according to Franck-Condon factors (FCF), which are nearly diagonal due to the Rydberg character (see Table 1). Predissociation occurs on a longer time scale, via non-adiabatic transition to a valence state. Thus the oxygen molecule dissociates with a KER given by the difference between the rovibrational energy level of the Rydberg state and the potential energy of the dissociative state at infinite internuclear distance, producing a sharp energy distribution. This component of the KER spectrum allows us to fully quantify the excitation of the ion.

All the peaks in the KER spectrum (Fig. 5) can be associated either to IDCE (a, b, c, e) or DDCE (d, f) [3, 4, 6]. Those processes are indicated below:

$$\begin{aligned}
\text{a}&: O_2(C\,^3\Pi_g, v''=0, N'') \rightarrow O(^3P) + O(^1D)\\
\text{b}&: O_2(d\,^1\Pi_g, v''=0, N'') \rightarrow O(^3P) + O(^1D)\\
\text{c}&: O_2(C\,^3\Pi_g, v''=1, N'') \rightarrow O(^3P) + O(^1D)\\
\text{d}&: \qquad\qquad\qquad\qquad O(^3P) + O(^1D)\\
\text{e}&: O_2(C\,^3\Pi_g, v''=0, N'') \rightarrow O(^3P) + O(^3P)\\
\text{f}&: \qquad\qquad\qquad\qquad O(^3P) + O(^3P).
\end{aligned}$$

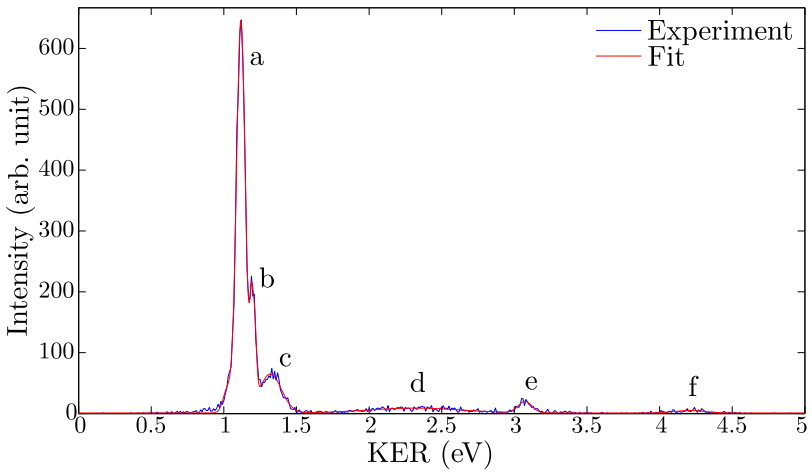

Figure 5. Experimental KER spectrum. Each peak is associated to a rovibrational state of O_2^+ and a dissociation channel (IDCE: a,b,c,e – DDCE; d,f).

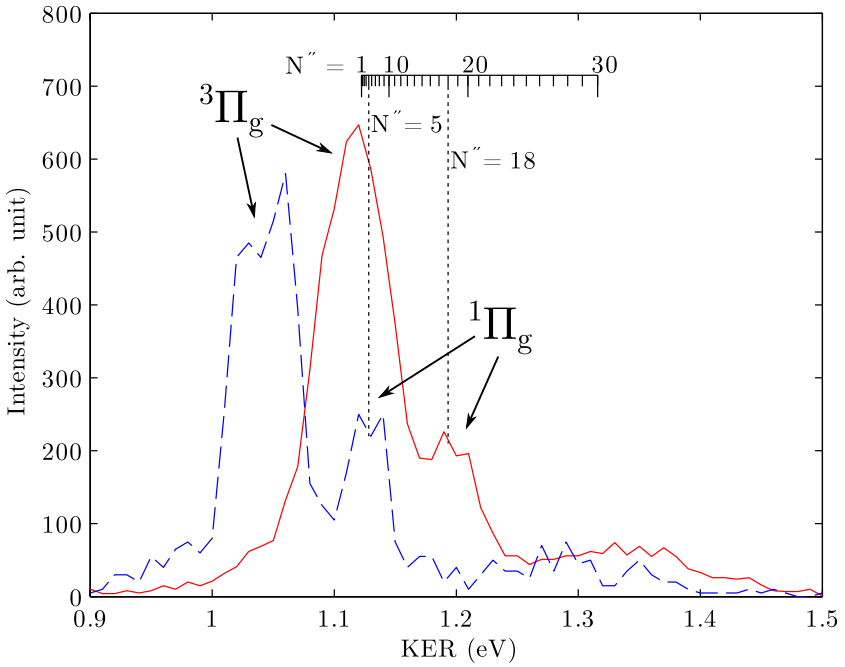

Figure 6. Examples of KER rotational shift. This figure is a zoom on two KER spectra taken at different wavelengths (blue dashed line: 301.250 nm, red full line: 300.249 nm), corresponding to $N'' \simeq N^+ \simeq N' = 5$ and 18 respectively. Those two spectra are similar in shape, but are shifted with respect to one another. This shift is caused by the rotational energy of the oxygen ion (ladder on top).

5. Rovibrational selectivity of the REMPI process

Finally, we have to confirm that the vibrational and rotational levels of the ion are sufficiently close to those of the intermediate state. This is performed by measuring the KER after DCE with K (see Sect. 4).

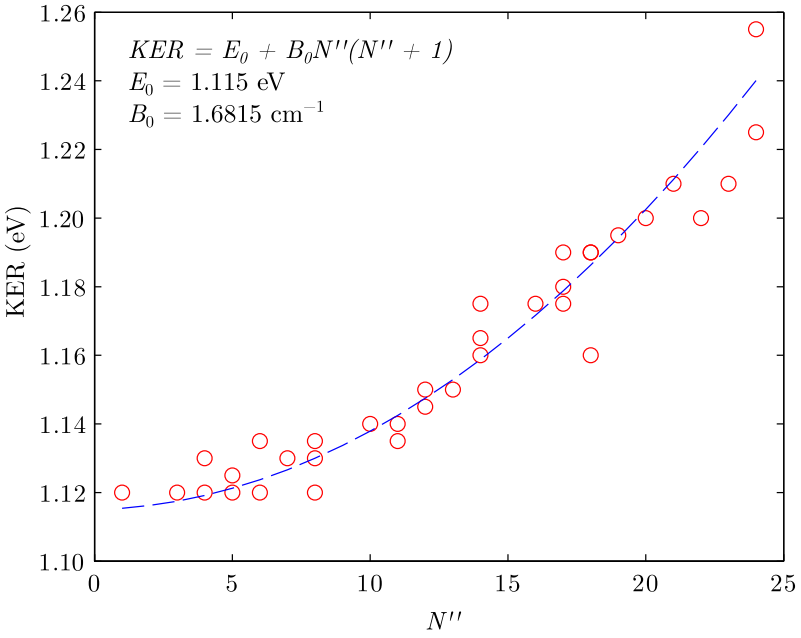

Figure 7. Determination of the rotational level by DCE. The red circles are the experimental values and the blue dashed line is the theoretical curve.

As seen in Fig. 5, the peaks associated to $O_2^+(X\,^2\Pi_g, v^+ = 0)$ dominate the spectrum, indicating that the vibrational level is qualitatively preserved. A clear contribution of the $v^+ = 1$ state is present however, which results from a two-step ionization process mediated by a core-excited state of O_2 crossing the O_2^+ ground state, along which the molecule starts to dissociate before autoionization takes place. Such a mechanism was already invoked by for the (3+1)REMPI of H_2 [11]. Note that free electron capture by O_2^+ to such an autoionizing state leads to dissociative recombination.

Individual rotational levels are not resolved in the KER spectrum shown in Fig. 6, however they induce a shift of the peaks which can be compared to theoretical predictions. We chose the peak associated to the $O_2(d\,^1\Pi_g, v'' = 0) \rightarrow O(^3P) + O(^1D)$ transition, since it has the smallest FWHM due to longer predissociation lifetime. The kinetic energy distribution was recorded at selected wavelengths throughout the REMPI spectrum corresponding to different, sometimes overlapping rotational branches. Multiple measurements were thus performed for the same intermediate N' level, while some specific N' values are missing due to excessive overlap. The good agreement between theory and experiment (Fig. 7) shows that the rotational level $N' \simeq N^+ \simeq N''$ is qualitatively preserved throughout the sequence of REMPI and electron capture, within the resolution of the measurement.

The theoretical curve simply follows the law $\mathrm{KER} = E_0 + B_0 N''(N''+1)$ with $E_0 = 1.115\,\mathrm{eV}$ and $B_0 = 1.6815\,\mathrm{cm}^{-1}$. The scatter of experimental points is caused by the resolution of the fit and the statistics of the measurements.

6. Conclusion

We have successfully shown that a rovibrationally selected O_2^+ beam may be produced by (2+1) REMPI. More specifically, we have excited the $d\,^1\Pi_g, v' = 0$ state of the neutral molecule, and identified all rotational branches in the photoionization yield. Then we have determined to which extent the vibrational state is preserved upon ionization, via dissociative charge exchange and precise KER

determination. The same method can be applied to obtain a rovibrationally selected $O_2^+(X\,^2\Pi_g)$ beam with $v^+ = 1, 2, 3$ [5]. In all cases, the proper selection of low angular momentum states will require the parent O_2 gas to be cooled by supersonic expansion, which raises the issue of unwanted collisions in the acceleration process, that may alter the selectivity of the REMPI technique. Such an effect has been discussed by Kreckel *et al.* [12] for H_3^+. The implementation of a laser ion source is foreseen for DR measurements at the CSR storage ring in Heidelberg, for direct injection of cold or selected ions of infrared inactive species.

The authors thank M. Génévriez for fruitful discussions. This work has been supported by the Fund for Scientific Research – FNRS through IISN contract No. 4.4504.10.

References

[1] J. L. Fox and A. Haé, J. Geophys. Res. **102**, 24,005-24,011 (1997)
[2] E. C. Zipf, J. Geophys. Res. **85**, 4232-4236 (1980)
[3] A. Petrignani, W. van der Zande, P. Cosby, C. F. Hellberg, R. Thomas and M. Larsson, J. Chem. Phys. **122**, 014302 (2005)
[4] W.J. van der Zande, W. Koot, J.R. Peterson and J. Los, Chem. Phys. Lett. **126**, 169-180 (1988)
[5] A. Sur, R.S. Friedman, and P. Miller, J. Chem. Phys. **94**, 1705 (1991)
[6] W.J. van der Zande, W. Koot, J.R. Peterson and J. Los, Chem. Phys. Lett. **140**, 175-180 (1987)
[7] G. Herzberg, *Spectra of diatomic molecules* (Van Nostrand, Princeton 1950)
[8] H. Lefebvre-Brion and R.W. Field, *Perturbations in the spectra of diatomic molecules* (Academic Press, Orlando 1986)
[9] H. Lefebvre-Brion and T. Ridley, J. Chem. Phys. **123**, 144306 (2005)
[10] Y. Li, I. Petsalakis, H-P. Liebermann, G. Hirsch and R. Buenker, J. Chem. Phys. **106**, 1123 (1997)
[11] S.N. Dixit, D. L. Lynch and V. McKoy, Phys. Rev. A **30**, 3332(R) (1984)
[12] H. Kreckel, O. Novotny, K.N. Crabtree, H. Buhr, A. Petrignani, B.A. Tom *et al.*, Phys. Rev. A **82**, 042715 (2010)